ACS OMEGA

http://pubs.acs.org/journal/acsodf

Article

First-Principles Study on Interlayer Spacing and Structure Stability of NiAl-Layered Double Hydroxides

Xiaoliang Wang,* Haonan Zhao, Leiming Chang, Zhenqiu Yu, Zhiwu Xiao, Shuwei Tang, Chuanhui Huang, Jingxin Fan, and Shaobin Yang*

Cite This: *ACS Omega* 2022, 7, 39169–39180

Read Online

ACCESS | Metrics & More | Article Recommendations

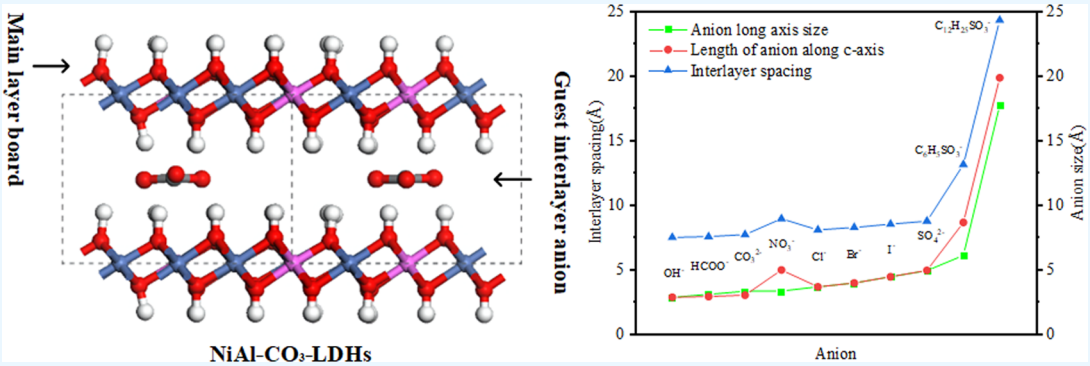

ABSTRACT: Interlayer spacing and structure stability of layered double hydroxides (LDHs) on their application performance in adsorption, ion exchange, catalysis, carrier, and energy storage is important. The effect of different interlayer anions on the interlayer spacing and structure stability of LDHs has been less studied, but it is of great significance. Therefore, based on density functional theory (DFT), the computational model with 10 kinds of anions intercalated Ni_3Al-A-LDHs (A = Cl^-, Br^-, I^-, OH^-, NO_3^-, CO_3^{2-}, SO_4^{2-}, $HCOO^-$, $C_6H_5SO_3^-$, $C_{12}H_{25}SO_3^-$) and four Ni_RAl-Cl-LDH models with different Ni^{2+}/Al^{3+} ratios (R = 2, 3, 5, 8) were constructed to calculate and analyze interlayer spacing, structural stability, and their influence factors. It was found that the interlayer spacing order of Ni_3Al-A-LDHs intercalated with different anions is $OH^- < CO_3^{2-} < Cl^- < Br^- < I^- < HCOO^- < SO_4^{2-} < NO_3^- < C_6H_5SO_3^- < C_{12}H_{25}SO_3^-$. The hydrogen bond network between the base layer and the interlayer anions affects the arrangement structure of the interlayer anions, which affects the interlayer spacing. For interlayer monatomic anions Cl^-, Br^-, and I^- and the anion of comparable size in each direction SO_4^{2-}, the interlayer spacing is positively correlated with the interlayer anion diameter. The larger difference between the long-axis and short-axis dimensions of the polyatomic anions results in the long axis of the anion being perpendicular to the basal layer, increasing interlayer spacing. The long-chain anion $C_{12}H_{25}SO_3^-$ intercalation system exhibits the largest layer spacing of 24.262 Å. As R value increases from 2 to 8, the interlayer spacing of Ni_RAl-Cl-LDHs gradually increases from 7.964 to 8.124 Å. The binding energy order between the interlayer anion and basal layer is $CO_3^{2-} > SO_4^{2-} > OH^- > Cl^- > Br^- > I^- > HCOO^- > NO_3^- > C_{12}H_{25}SO_3^- > C_6H_5SO_3^-$. The smaller the interlayer spacing, the higher the binding energy and the stronger the structural stability of LDHs. The factors affecting structural stability mainly include the bond length and bond angle of the hydrogen bond and the charge interaction between the basal layer and interlayer anion. In the CO_3^{2-} intercalated system, the hydrogen bond length exhibits the shortest of 1.95 Å and the largest bond angle of 163.68°. The density of states and energy band analysis show that the higher the number of charges carried by the anion, the stronger its ability to provide electrons to the basal layer.

1. INTRODUCTION

Layered double hydroxides (LDHs) are a kind of two-dimensional (2D) material. The interlayer guest anion has a negative charge and plays a decisive role in the construction and functional regulation of the host and guest functional materials. For different functional LDH materials, interlayer anions can be adjusted by ion exchange and other methods. The same anion can be intercalated into the interlayer of different basal layers. Therefore, due to the interchangeability of the basal layer cation

Received: August 8, 2022
Accepted: October 5, 2022
Published: October 21, 2022

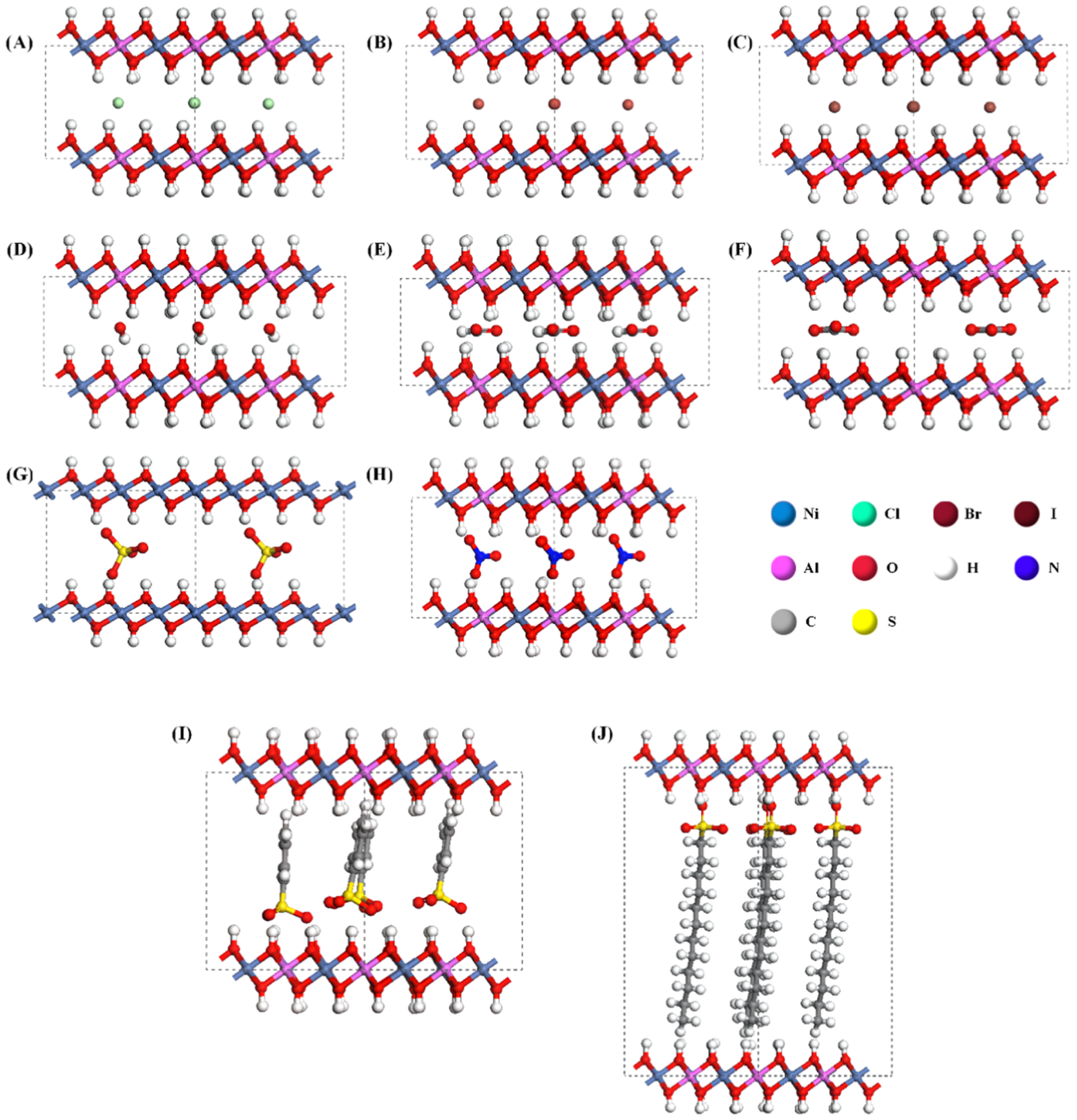

Figure 1. Structural models of NiAl-A-LDHs with different interlayer anions. (A) NiAl-Cl-LDHs; (B) NiAl-Br-LDHs; (C) NiAl-I-LDHs; (D) NiAl-OH-LDHs; (E) NiAl-HCOO-LDHs; (F) NiAl-CO_3-LDHs; (G) NiAl-SO_4-LDHs; (H) NiAl-NO_3-LDHs; (I) NiAl-$C_6H_5SO_3$-LDHs; (J) NiAl-$C_{12}H_{25}SO_3$-LDHs.

and guest anion in LDHs, LDHs exhibit significant potential for applications in the fields of catalysis,[1,2] adsorption,[3,4] ion exchange,[5,6] biomedicine,[7] light and magnetism,[8] and other functional materials fields and have received widespread attention from academia and industry.[9]

The functional properties of LDHs mentioned above are influenced by the guest anion and cation in the basal layer, as well as by the interlayer spacing and the stability of the architecture.[10] Designing and regulating the interlayer spacing structure has become an essential topic in the research of LDH materials. Fruitful results have been achieved using experimental methods to modulate the interlayer spacing, such as changing the interlayer spacing and structural stability[10−12] by adjusting the anion size and type[13−16] and regulating the basal layer metal element ratio and synthesis conditions to improve functional properties.[17−19] NiAl-LDHs have many research reports on electricity storage, catalysis, adsorption, etc., and are expected to achieve industrial application.[20−22] The effects of anion intercalation of CO_3^{2-}, NO_3^-,[23] Cl^-,[24] sodium dodecyl sulfate,[25] etc., on the interlayer spacing of NiAl-LDHs have all shown that large interlayer spacing has a positive effect on supercapacitor and catalytic performances. However, the

https://doi.org/10.1021/acsomega.2c05067
ACS Omega 2022, 7, 39169−39180

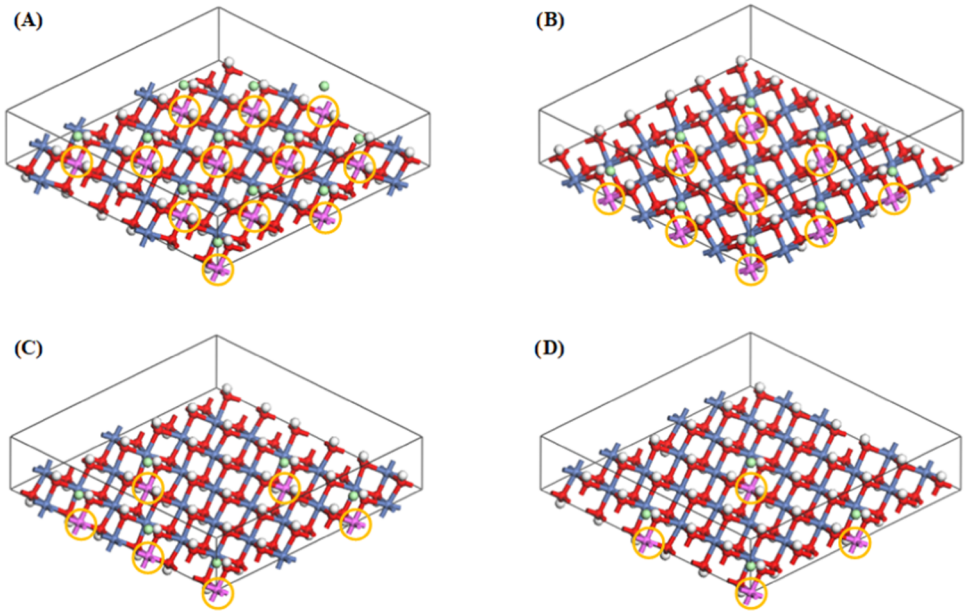

Figure 2. Structural models of Ni_RAl-Cl-LDHs with different Ni/Al ratios (R). (A) R = 2; (B) R = 3; (C) R = 5; (D) R = 8 (the orange circles are marked with Al ions).

microscopic mechanisms affecting the layer spacing and stability of NiAl-LDHs were not systematically reported. It is not easy to experimentally investigate the nature of supermolecular interactions between metal cations and hydroxyl groups on the basal layers of LDHs[26] or between basal layers and guests.[27,28] But it is very convenient to calculate these crystal properties using the plane-wave pseudopotential method of density functional theory (DFT) and periodic boundary conditions. Many valuable results have been obtained from the density functional theory study of LDHs. For example, Costa[29] used the DFT method to calculate and discovered that the interlayer spacing of carbonate intercalation of Zn-Al- and Mg-Al-LDHs are lower than chloride anions, showing that carbonate interacts more strongly with the basal layer of LDHs compared to chloride anions. Xia et al.[30] calculated and analyzed the properties of Mulliken charge population, hydrogen bonding, the density of states (DOS), etc., by DFT, and explained and compared the differences in the structural stability of LDHs. The results demonstrate that the photocatalytic performance of LDHs with different interlayer anions is highly correlated with their structural stability. Lv et al.[1] calculated properties such as geometric parameters, charge population, and binding energy by DFT; explored the effects of different divalent metal cations on the structure and stability of CuMgAl-LDHs, etc.; and obtained the results that the order of chemical structure stability is CuMgAl > CuZnAl > CuNiAl; however, the order of photocatalytic activity is reversed. Liu et al.[28] used the DFT method to analyze that the guest anion plays a key role in the construction of LDH materials by constructing the MgAl-A-LDH model in terms of binding energy, the density of states, and differential charge density. Zhao et al.[31] investigated the ion exchangeability in different LDHs with the same charge anion by the $Dmol_3$ and Forcite modules. However, the effect of interlayer anion occupancy and arrangement on interlayer spacing has not been thoroughly investigated. There are few articles about the interlayer spacing and structural stability of Ni-Al-LDHs using the computational simulations method.

This paper mainly adopted the first-principles method based on DFT to calculate the factors influencing interlayer spacing and structural stability. We constructed the computational model Ni_3Al-A-LDHs intercalated with 10 kinds of anions (A = Cl^-, Br^-, I^-, OH^-, NO_3^-, CO_3^{2-}, SO_4^{2-}, $HCOO^-$, $C_6H_5SO_3^-$, $C_{12}H_{25}SO_3^-$) and four Ni_RAl-Cl-LDH models with different Ni^{2+}/Al^{3+} ratios (R = 2, 3, 5, 8) to analyze binding energy, differential charge density, charge population, and the DOS and band gap of LDHs intercalated by different anions, for revealing the influence mechanism of interlayer anions types, diameter, number, occupancy and arrangement, and the number of positive charges in a basal layer on the interlayer spacing of LDHs, to explore the structural stability laws of Ni_3Al-LDHs with different interlayer anions inserted, and to provide a theoretical basis for further research on LDH materials.

2. COMPUTATIONAL DETAILS

2.1. Modeling of LDHs. The stacking sequences of the layers of LDHs include three types: three-layer rhombohedral polytype (3R), two-layer hexagonal polytype (2H), and one-layer hexagonal polytype (1H). The most common types of LDH stacking are 3R and 2H. The 3R construct is the stable stacking mode for the same basal layer cation ratio. However, the three stacking methods have no significant effect on the layer spacing and interlayer ions, and 1H has a smaller period and can be widely adopted by significantly saving computational resources.[28] This paper employs the models of the LDH basal layer with the 1H stacking method. The space group is $P\bar{3}M1$ (no. 164); lattice parameters are $\alpha = \beta = 90°$ and $\gamma = 120°$; and a, b, and c are referred to as powder X-ray diffraction (XRD) data corresponding to LDHs.[32,33] The c of the cell parameter is a parameter reflecting interlayer spacing, which is influenced by the ratio of interlayer anions to basal layer cations. To investigate the effect of the interlayer anion and basal layer cation ratio on the interlayer spacing of LDHs, we constructed Ni_3Al-A-LDH models intercalated by 10 kinds of anions (A = Cl^-, Br^-, I^-, OH^-, NO_3^-, CO_3^{2-}, SO_4^{2-}, $HCOO^-$, $C_6H_5SO_3^-$, $C_{12}H_{25}SO_3^-$ (Figure 1)) and four Ni_RAl-Cl-LDH models with different Ni^{2+}/

https://doi.org/10.1021/acsomega.2c05067
ACS Omega 2022, 7, 39169−39180

Table 1. Structural Composition, Geometrical Parameters, Energy Values, and Anion Long- and Short-Axis Dimensions of Different Interlayer Anions Ni_3Al-LDHs (A = Cl^-, Br^-, I^-, OH^-, NO_3^-, CO_3^{2-}, SO_4^{2-}, $HCOO^-$, $C_6H_5SO_3^-$, $C_{12}H_{25}SO_3^-$)

anion	formula	C_{Ref} [31,32,40] (Å)	C_{Cal} (Å)	energy (eV)	E_B [a] (eV)	L/S [b] (Å)
Cl^-	$Ni_{12}Al_4(OH)_{32}Cl_4$	7.86	8.028	−33 174.78	−9.34	3.62/3.62
Br^-	$Ni_{12}Al_4(OH)_{32}Br_4$	7.95	8.219	−33 335.32	−8.19	3.92/3.92
I^-	$Ni_{12}Al_4(OH)_{32}I_4$	8.16	8.474	−34 657.32	−7.88	4.4/4.4
OH^-	$Ni_{12}Al_4(OH)_{32}(OH)_4$	7.55	7.447	−33 301.44	−10.31	2.8/2.22
NO_3^-	$Ni_{12}Al_4(OH)_{32}(NO_3)_4$	8.79	8.895	−37 822.48	−5.82	3.3/2.8
CO_3^{2-}	$Ni_{12}Al_4(OH)_{32}(CO_3)_2$	7.65	7.670	−34 421.87	−24.95	3.28/2.8
SO_4^{2-}	$Ni_{12}Al_4(OH)_{32}(SO_4)_2$	8.58	8.705	−35 583.72	−21.34	4.88/4.88
$HCOO^-$	$Ni_{12}Al_4(OH)_{32}(HCOO)_4$	7.2	7.507	−35 670.74	−6.18	3.04/2.8
$C_6H_5SO_3^-$	$Ni_{12}Al_4(OH)_{32}(C_6H_5SO_3)_4$	13	13.096	−42 041.21	−3.82	6.05/4.93
$C_{12}H_{25}SO_3^-$	$Ni_{12}Al_4(OH)_{32}(C_{12}H_{25}SO_3)$	24	24.262	−47 116.45	−5.34	17.7/5.29

[a] E_B represents the binding energy of the LDH system with different anion insertion. The detailed calculation formula is shown in Section 3.2. [b] L and S represent, respectively, the anion long- and short-axis dimensions of LDHs.

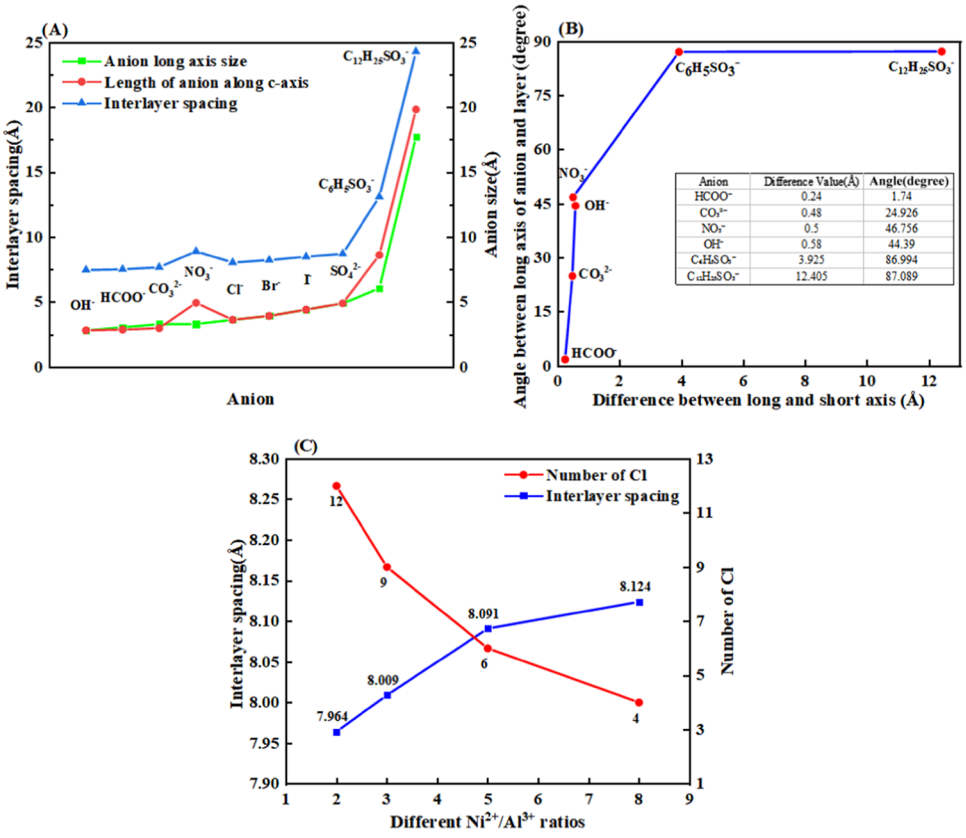

Figure 3. (A) Comparison of interlayer spacing, ion long-axis dimensions, and ion dimensions along c-axis for different interlayer anions Ni_3Al-A-LDHs; (B) plots of difference between long and short axes of interlayer polyatomic anions and relationship between the long axis and angle of laminate; (C) comparison of effects of interlayer spacing and the number of chloride ions for different Ni−Al ratios of LDHs.

Al^{3+} ratios (R = 2, 3, 5, 8 (Figure 2)). The periodical supercell is 4 × 4 × 1 in the a-, b-, and c-directions. The optimized model structure is shown in Figure 1. The basal layer's composite metal hydroxide octahedra always maintain the octahedral structure. Following the calculation of the lowest energy permutation of the Cl anion by Xu et al.,[34] interlayer intercalation anions are uniformly distributed directly below Al ions in the middle of two basal layers.

2.2. Computational Methods. All of the calculations were implemented with the CASTEP module based on DFT in the Materials Studio. Structural stability and the electronic structure were performed using the pseudopotential plane-wave method. Exchange−correlation energy was calculated by the Perdew−Burke−Ernzerhof (PBE)[35] -generalized functions under the generalized gradient approximation (GGA)[36,37] to obtain the structure of LDHs at the lowest energy. Structural geometry optimization and property calculation of NiAl-A-LDHs were at the basis group level. The convergence target of the interatomic force was 0.01 eV/Å. The energy convergence accuracy of self-consistent cycle calculation was set to 5.0×10^{-5} eV/atom. The internal crystal stress convergence target was set to 0.2 GPa. The maximum atomic displacement convergence target was set to 0.005 Å. Plane-wave cutoff energy was 381 eV. The DFT dispersion correction is used with the Tkatchenko−Scheffler (TS) method to describe noncovalent forces, such as hydrogen bonds, electrostatic gravity, and van der Waals interactions,

https://doi.org/10.1021/acsomega.2c05067
ACS Omega 2022, 7, 39169−39180

essential for the formation, stability, and function of molecules and materials. Ionic nuclei were described by the modified ultrasoft pseudopotentials (OTFG ultrasoft pseudopotentials) to increase metastability and reduce the number of plane waves required for Kohn−Sham orbital expansion for describing the interactions between valence electrons and ions. The Broyden−Fletcher−Goldfarb−Shanno (BFGS) algorithm is used to search for potential energy surfaces during optimization, geometric optimization lattice constants, and atomic coordinates of structural models to obtain models with minimum total energy and most stable states. To compute the density of states (DOS) of Ni_RAl-A-LDHs, the Γ-point-centered *k*-point meshes used for Brillouin zone integration were set as 2 × 2 × 3. The self-consistent field calculation error was 1.0×10^{-5} eV/atom. Base state energy was calculated by selecting the Pulay density mixing algorithm. The overall charge count was set to 0. The spin polarization and Hubbard correction (DFT + *U*)[38] must also be considered in the simulation calculations of LDHs. In particular, the structural system of LDHs involves transition-metal elements. There are strong electronic interactions due to the presence of transition-metal elements. It is fixed in the literature using Hubbard *U* for corrected calculations based on DFT. So, the spin polarization was set, $U_{Ni}^{2+} = 3.8$ eV,[32,38,39] and the other atoms have their *U* values set to 0.[38] Meanwhile, cell optimization was selected to optimize cells, and other parameters were set to default values.

3. RESULTS AND DISCUSSION

3.1. Effect of Anion and Basal Layer Charge on Interlayer Spacing. *3.1.1. Interlayer Spacing Characteristic.* The interlayer spacing is one of the principal indicators for structural analysis of LDHs. Experimentally, the values of the interlayer spacing of LDHs are often obtained by XRD measurements. In the calculation model, the *c* value reflects the dimension of the interlayer spacing. Combined with the literature of experimental studies, it can be determined that the long-chain guests between layers of LDHs are mostly arranged vertically or close to vertically with the basal layer.[40−42] Therefore, in the original model, the anions are arranged between layers perpendicular to the basal layer in the long-axis direction. After structural optimization, the placement state of each anion in the LDH interlayer is shown in Figure 1. The geometric optimization results show that the interlayer anions greatly influence the unit cell parameter *c* but have little influence on *a* and *b*. *a* and *b* are almost unchanged during the optimization process. *c* values in the optimized results of the Ni_3Al-LDH model with different interlayer anions are shown in Table 1 and are similar to the literature. The result shows that with the same Ni/Al ratio *R* of 3 for each LDH model, the interlayer spacing increases in the order of $OH^- < CO_3^{2-} < Cl^- < Br^- < I^- < HCOO^- < SO_4^{2-} < NO_3^- < C_6H_5SO_3^- < C_{12}H_{25}SO_3^-$. According to the literature, it is known that the main factors affecting the interlayer spacing of LDHs are the interlayer anion[43] and the basal layer cation ratio.[44] For interlayer monatomic anions Cl^-, Br^-, and I^- and anions of comparable size in each direction SO_4^{2-}, the interlayer spacing is positively correlated with the interlayer anion diameter. This assertion is consistent with the literature.[28] When polyatomic anions with inconsistent dimensions in all directions exist between layers, for example, OH^-, NO_3^-, CO_3^{2-}, $HCOO^-$, $C_6H_5SO_3^-$, and $C_{12}H_{25}SO_3^-$, the interlayer spacing loses significant correlation with dimensions in directions other than the long axis of the anion, still has some correlation with the long-axis dimensions of the anion (Figure 3A). However, there are some unrelated exceptions, such as NO_3^-. Under the condition of NO_3^- intercalation, the interlayer spacing and the size of interlayer NO_3^- along the *c*-axis show a relatively strict positive correlation. Moreover, the interlayer spacing of all anions after intercalation has a better positive correlation with the size of the anions along the *c*-axis direction. It shows that the size of the interlayer anion along the *c*-axis direction ($SIZE_C$) is the only factor result in the interlayer spacing when the basal layer composition and the ion ratio are the same. Combined with Figure 1, it can be seen that $SIZE_C$ is influenced by the anion configuration and the number of aggregates. Therefore, measuring long-axis dimensions, short-axis dimensions, and the angle between the long-axis and the basal layer of polyatomic anions can explain these interlayer anion arrangement configurations, aggregation states, $SIZE_C$, and the effect on the interlayer spacing.

3.1.2. Effect of Interlayer Anion Type, Number, and Configuration on Interlayer Spacing. Measuring results of the long-axis dimension, short-axis dimension, and the angle between the long axis and the basal layer for polyatomic anions such as OH^-, $HCOO^-$, $C_6H_5SO_3^-$, $C_{12}H_{25}SO_3^-$, and CO_3^{2-} are shown in Figure 3B. The larger the difference between an anion's long-axis and short-axis dimensions, the more the ion tends to be arranged perpendicular to the basal layer. CO_3^{2-}, OH^-, and $HCOO^-$ have small angles with the basal layer. Among them, the difference between the long axis and the short axis of $HCOO^-$ is the smallest, only 0.24 Å, and the angle between its long axis and the basal layer is 1.74°, which is also the smallest, almost parallel to the basal layer, while $C_6H_5SO_3^-$ and $C_{12}H_{25}SO_3^-$ are close to perpendicular to the basal layer. The long axis of $C_{12}H_{25}SO_3^-$ has the longest dimension and the largest difference from the short axis, with 12.4 Å, and the angle with the basal layer reaches 87.1°. It is concluded that for the polyatomic anions between LDH layers, the greater the difference between their long- and short-axis dimensions, the more the anions tend to be perpendicular to the LDH basal layer, causing the larger interlayer spacing of LDHs for long-chain anion intercalation (Figure 3A). The interlayer spacing of LDHs depends on the interlayer anion configuration and the number of aggregates. It is essentially determined by hydrogen bonding characteristics and system energy between the basal layer and interlayer anions or between anions and anions. The system will spontaneously evolve in the direction of forming as many hydrogen bonds as possible. Many hydrogen bonds are formed in the system, the system energy is low, and the system's structure remains more stable.[45]

The number of hydrogen bonds formed by oxygen atoms in NO_3^-, CO_3^{2-}, OH^-, $HCOO^-$, and SO_4^{2-} with hydrogen atoms in the hydroxyl group of LDHs on both sides is higher than that formed by hydrogen atoms in the hydroxyl group of LDH on one side. The number of hydrogen bonds formed is large, and the system exhibits lower energy. So, the system spontaneously drives the oxygen atoms in the anions to be close enough to the hydroxyl hydrogen atoms of both sides' basal layers to reach the distance to form hydrogen bonds. Therefore, theoretically, NO_3^-, CO_3^{2-}, OH^-, $HCOO^-$, and LDH basal layers exist in a conformational arrangement with small pinch angles. However, the angle between NO_3^- and LDH basal layer is 46.8° and does not show a structure parallel to the LDH basal layer (Figure 1) due to the electrostatic repulsion between NO_3^- in the case of the amount of NO_3^-. To balance the positive charge carried by the LDH basal layer, the number of negative monovalent anions

https://doi.org/10.1021/acsomega.2c05067
ACS Omega 2022, 7, 39169−39180

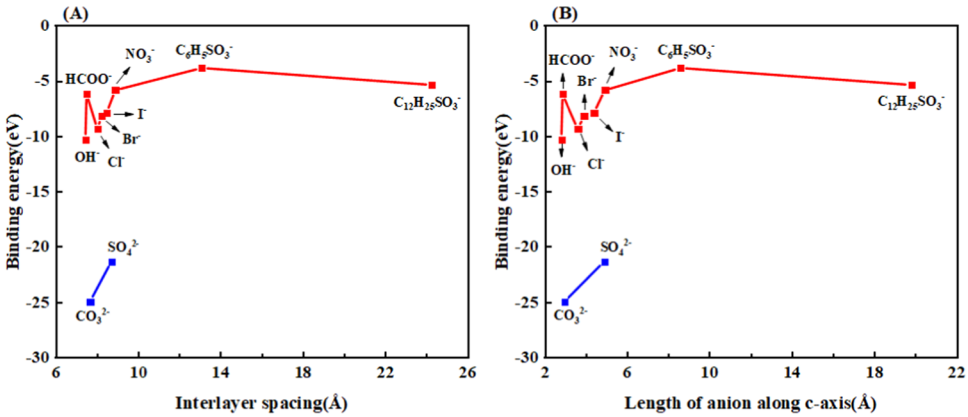

Figure 4. Comparison of the binding energy of different interlayer anion Ni_3Al-A-LDH (A = Cl^-, Br^-, I^-, OH^-, NO_3^-, CO_3^{2-}, SO_4^{2-}, $HCOO^-$, $C_6H_5SO_3^-$, $C_{12}H_{25}SO_3^-$) model systems; (A) interlayer spacing vs binding energy; (B) anion size along the *c*-axis vs binding energy.

such as Cl^- and NO_3^- inserted interlayers is twice as much as the negative divalent anions such as CO_3^{2-} and SO_4^{2-}. Under the electrostatic repulsion between the O atoms surrounding the N atoms in NO_3^- anions, NO_3^- deviates from a dense parallel arrangement, resulting in increased size along the *c*-axis and increased interlayer spacing. Similar results were obtained in the literature.[28,46]

The monatomic anions Cl^-, Br^-, and I^- are arranged in a plane between the layers, and all form hydrogen bonds with the adjacent basal layers (Figure 1). Since the electronegativity of Cl, Br, and I atoms decreases sequentially, the radii of Cl^-, Br^-, and I^- ions increase sequentially, resulting in the formation of longer hydrogen bonds, which lead to an increase in the interlayer spacing. There is hydrogen bonding between $HCOO^-$ and hydrogen atoms on the surface of the basal layer. Thus, a high density of $HCOO^-$ keeping the arrangement parallel to the basal layer is the lowest energy configuration, resulting in smaller $SIZE_C$ and interlayer spacing. The oxygen atoms of SO_4^{2-} are located at each top corner of the tetrahedral structure. Due to the symmetry, upright and upside-down SO_4^{2-} in interlayers are the same structure, with the same number of hydrogen bonds and energy. Therefore, the LDH interlayer spacing of SO_4^{2-} intercalated is highly correlated with the height of the tetrahedral structure of SO_4^{2-}. All O atoms of $C_6H_5SO_3^-$ and $C_{12}H_{25}SO_3^-$ are located at one end of the long chain and can form hydrogen bonds with hydrogen atoms on the surface of the basal layer, either parallel or perpendicular to it. When the long-chain anions among the layers are very few, the long-chain anions parallel to the basal layers can form more hydrogen bonds, with the minimum system energy.[47,48] However, when there are many long-chain anions between the layers, the long-chain anions in the middle position cannot form hydrogen bonds with the basal layer due to stereoscopic obstruction, and the system structure is unstable. Long-chain anions are transformed perpendicular to the basal layer to form sufficient hydrogen bonds to obtain minimum system energy. In this paper, when the ratio of divalent and trivalent cations of the LDH basal layer $R = 3$, the number of interlayer anions required to balance the positive charge of the basal layer is higher. In the limited space between the layers of LDHs, the electrostatic repulsion among the anions will keep the anions at a certain distance from each other. Supposing the long-chain of anions is arranged parallel to the plating layer, the long-chain anions will be arranged in three or four layers, and the oxygen atoms in the middle layer of anions are far away from the LDH basal layer and cannot form hydrogen bonds. The anion conformation tends toward forming a high number of hydrogen bonds for low system energy. Meanwhile, the long-chain anions are simultaneously subjected to the interaction of densely arranged neighboring anions.

3.1.3. Effect of the Cation Ratio in the Basal Layer on Interlayer Spacing. In addition to the intercalating anions, the interlayer spacing is closely related to the positive charge of the basal layer. To study the variation of interlayer spacing with the number of positive charges on the basal layers, computational models Ni_RAl-Cl-LDHs were constructed for the ratios *R* of 2, 3, 5, and 8 using chloride ions as interlayer intercalation guests to exclude the effects of dimensions in different directions for interlayer anions. After structural geometry optimization, the position of the interlayer chloride anions did not change, always located in the middle of the two basal layers and directly below the aluminum ions, which indicates that the interlayer anion does not affect the structure of basal layers. From Figure 3C, we found that the interlayer spacing gradually increases as the *R* value increases. One reason is as the *R* value increases, the concentration of positive charge from Al^{3+} in the basal layer decreases, resulting in a weaker electrostatic force between the base layer and chloride anions and an increase in the interlayer distance. On the other hand, as the *R* value increases, the number of interlayer chloride anions that balance the positive charge of the basal layer gradually decreases, and the number of hydrogen bonds between chloride anions and the basal layer reduces, resulting in weakening of the interlayer force and an increase in the interlayer distance. Thus, the LDH interlayer spacing is not only related to the ionic size, structure, charge carried, and placement state of the guest anion but also depends on the ratio of metal cations, i.e., the number of positive charges, in the LDH basal layer.

3.2. Structural Stability Analysis of Ni_3Al-LDHs.

3.2.1. Effect of Interlayer Anion and Interlayer Spacing on Binding Energy. The binding energy of basal layers and interlayer anions can reflect the strength of the anion exchange capacity and the stability of object intercalation structure between the different layers. The average binding energy (E_B) of anions in NiAl-A-LDHs was calculated as follows[31]

$$E_B = \frac{(E_{LDHs} - E_{Layer}) - N_A E_A}{N_A}$$

where E_{LDHs} represents the total energy of the Ni_3Al-LDH system, E_{Layer} represents the basal layer energy of the Ni_3Al-LDH system without anion insertion, N_A represents the number of

https://doi.org/10.1021/acsomega.2c05067
ACS Omega 2022, 7, 39169−39180

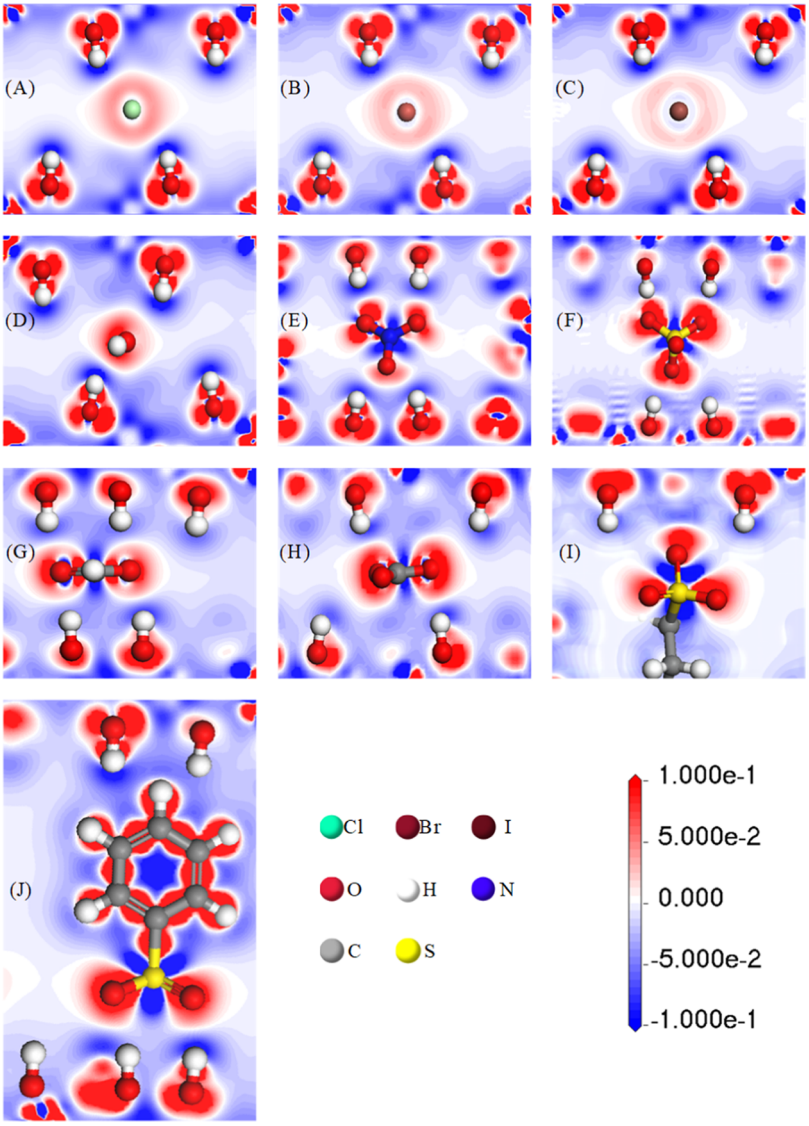

Figure 5. Differential charge density plots of different interlayer anion Ni_3Al-A-LDH model systems. (A) Ni_3Al-Cl-LDHs; (B) Ni_3Al-Br-LDHs; (C) Ni_3Al-I-LDHs; (D) Ni_3Al-OH-LDHs; (E) Ni_3Al-NO_3-LDHs; (F) Ni_3Al-SO_4-LDHs; (G) Ni_3Al-HCOO-LDHs; (H) Ni_3Al-CO_3-LDHs; (I) Ni_3Al-$C_{12}H_{25}SO_3$-LDHs; (J) Ni_3Al-$C_6H_5SO_3$-LDHs.

interlayer anions, and E_A represents the energy of a single interlayer anion. Binding energy calculation results are shown in Figure 4. It can be seen that the binding energy of divalent anions is significantly greater than that of monovalent anions. The binding energies of anions with the same charge differ little, fluctuating in several eV ranges. The binding energies of the systems intercalated with negative monovalent and negative divalent anions differ by 10 eV, and the difference is even larger, which shows that the binding energy is significantly affected by the charge number carried by the interlayer anion. The higher the number of electrons carried by the interlayer anion, the higher the binding energy, and the greater the structural stability of LDHs, the stronger the force between the interlayer anion and the LDH basal layer. Thus, anions with higher negative charge numbers are more likely to exchange for less-charged anions in the interlayer region of LDHs. The order of the binding energy of the interlayer anions to the basal layer of LDHs is CO_3^{2-} > SO_4^{2-} > OH^- > Cl^- > Br^- > I^- > $HCOO^-$ > NO_3^- > $C_{12}H_{25}SO_3^-$ > $C_6H_5SO_3^-$. This order demonstrates that the presence of interlayer carbonate anions makes LDHs the most stable structure. Because the carbonate remains parallel to the LDH basal layer after structural geometry optimization, the hydrogen bonds formed between the three O atoms of the carbonate and hydroxyl groups of the basal layer make this conformation more stable.[49]

Comparison of the trends of the binding energy of the intercalation system for the negative monovalent anions Cl^-, Br^-, I^-, OH^-, NO_3^-, etc., is shown in Figure 4A. It is found that the binding energy increases slowly with the decrease of the interlayer spacing. The trend of the binding energy of the intercalation system of negative divalent anions CO_3^{2-} and SO_4^{2-} also shows the same pattern. This indicates that the smaller the value of c, the stronger the interaction between the basal layer and the intercalating anion.[50] When the number of charges carried by the anion increases, its binding energy increases rapidly. The more stable the structural system is, the more difficult it is to exchange out from the LDH interlayer, while the lower the number of charges, the lower the binding energy, and the LDH structure becomes less stable, resulting in the anion being exchanged from the interlayer more easily.

https://doi.org/10.1021/acsomega.2c05067
ACS Omega 2022, 7, 39169−39180

$HCOO^-$ is a particular case. Its interlayer spacing is small, but the binding energy is slightly smaller than those of Cl^-, Br^-, and I^- intercalated Ni_3Al-LDHs. The reason is that the hydrogen bonding between $HCOO^-$ molecules weakens the hydrogen bonding strength between $HCOO^-$ and the hydrogen atom of the hydroxyl group of the basal layer, reducing the binding energy.

The plot of anion size vs binding energy along the *c*-axis in Figure 4B is similar to the plot of interlayer spacing vs binding energy in Figure 4A. For negative monovalent anions, the binding energy is related to the size of the anion in the interlayer along the *c*-axis direction, where the OH^- anion has a length of 2.81 Å along the *C*-axis and the binding energy of −10.31 eV. This indicates that the smaller the size along the *c*-axis of an anion of the same charge, the greater the binding energy of LDHs. For LDHs with $C_6H_5SO_3^-$ ion intercalation, its binding energy is smaller than those of the other anions due to the greater degree of electrostatic repulsion between the inserted $C_6H_5SO_3^-$ ions.[33] The negative divalent anion also shows the same pattern. In comparison, the binding energy of CO_3^{2-} was the largest, and that of SO_4^{2-} was the smallest, at −24.95 and −21.34 eV, respectively. This is the same result as in Liu et al.,[28] who studied the binding energy of different anion-intercalated MgAl-LDHs.

3.2.2. Structural Stability Analysis Using Differential Charge Density. The more the negative charges of interlayer anions, the higher the binding energy of LDHs, reflecting the charge density distribution of interlayer anions and basal layer atoms. From the electron density difference, the electron transport process and the interaction mode between the basal layer cation and interlayer anion can be obtained, which can explain the influence of the anion charge number on the binding energy. The results of electron density difference obtained by calculation are shown in Figure 5. The region of high electron density is red, and the region of low electron density is blue. From Figure 5, it can be seen that both the red area around the anion and the blue area around the hydrogen ion in the hydroxyl group of the basal layer produce contact, indicating that the interlayer anions have hydrogen bond production with both the basal layers. The higher the density of the red region in touch with each other or the blue region, the greater the difference in charge density between the two sides, indicating stronger hydrogen bonding and stronger interaction between the basal layer and the interlayer anion. For example, for the negative divalent anions CO_3^{2-} and SO_4^{2-} in oxygen, the density of the electron red region is higher, and the blue area around the hydrogen ions in the basal layer is also denser, indicating strong local hydrogen bonding and exhibiting high binding energy. When the intercalating anion is OH^-, due to its smallest diameter, it is closer to the hydrogen ions in the hydroxyl groups in the basal layer and has more charge transfer. Thus, LDHs with intercalated OH^- have the smallest interlayer spacing and the largest binding energy in univalent anions. The electron density difference plots of LDH basal layers far from the anion are similar, indicating that the interlayer guest anion has almost no effect on the charge transfer in the outer basal layer of LDHs.

3.2.3. Structural Stability Analysis Using Hydrogen Bonds. The strength of interlayer forces can also be determined from the hydrogen bonds' bond lengths and angles. The bond lengths and bond angles counted are shown in Table 2. The hydrogen bond length is mainly in the range of 1.42−2.7 Å, indicating the prevalence of hydrogen bonding interactions between the interlayer anions and the basal layers of LDHs.[51] It is well known that the shorter the bond length of a hydrogen bond and the closer the bond angle to 180°, the better the structural stability.[52] When divalent anions such as CO_3^{2-} are inserted between the layers of LDHs, the hydrogen bonds exhibit the shortest bond length of 1.95 Å. In addition, the CO_3^{2-} intercalated structure has the largest hydrogen bonding angle of 163.68°. Therefore, CO_3^{2-} intercalated LDHs have the strongest stability, consistent with the binding energy analysis. When the halogen anions are inserted among the layers, the bond length of the hydrogen bond gradually increases as the electronegativity of halogen decreases (Cl > Br > I), which is consistent with the binding energy sequence. When the interlayer is inserted with an oxygenate-containing anion, the OH^- ion has the smallest hydrogen bond length of 1.87 Å, and its binding energy value is the largest among all negative monovalent anions.

Table 2. Average Bond Lengths and Average Bond Angles of Individual Hydrogen Bonds in Ni_3Al-A-LDHs

Ni_3Al-A-LDHs	$L_{O-H\cdots X}$ (Å)	$\theta_{O-H\cdots X}$ (degree)
Ni_3Al-Cl-LDHs	2.47	150.06
Ni_3Al-Br-LDHs	2.57	143.73
Ni_3Al-I-LDHs	2.67	148.28
Ni_3Al-OH-LDHs	1.87	159.59
Ni_3Al-HCOO-LDHs	1.88	160.47
Ni_3Al-NO_3-LDHs	2.06	154.88
Ni_3Al-SO_4-LDHs	1.951	153.58
Ni_3Al-CO_3-LDHs	1.95	163.68
Ni_3Al-$C_6H_5SO_3$-LDHs	1.95	160.33
Ni_3Al- $C_{12}H2_5SO_3$-LDHs	1.8	148.77

3.2.4. Structural Stability Analysis Using Mulliken Charge Population. Mulliken charge population is an approach to characterize the charge distribution within each molecule in a structure and can be used to estimate the covalent and ionic bonding capacity of each molecule.[53] The method indirectly discusses the strength of intramolecular interactions and can reflect the interaction forces and the charge transfer of the LDH system. The larger the population value, the more the covalent bonding components, while the smaller the population value, the more the ionic bonding components. To further investigate the interaction between basal layers and anions in Ni_3Al-A-LDHs, charge population analysis was performed on Ni_3Al-A-LDHs, obtained the residential value of LDH basal layers and interlayer anions and is shown in Table 3. It can be seen that the Mulliken population values of LDH basal layers with different anion insertion decrease compared to that of LDH basal layers

Table 3. Mulliken Charge Population of Different Interlayer Anion NiAl-A-LDH Model Systems

Ni_3Al-A-LDHs	Q(A)/e	Q(Layer)/e
Ni_3Al-LDHs		4.00
Ni_3Al-OH-LDHs	−2.44	1.88
Ni_3Al-Cl-LDHs	−2.84	2.72
Ni_3Al-Br-LDHs	−2.32	2.12
Ni_3Al-I-LDHs	−2.16	2.12
Ni_3Al-NO_3-LDHs	−3.00	3.24
Ni_3Al-HCOO-LDHs	−3.24	3.68
Ni_3Al-CO_3-LDHs	−2.96	1.58
Ni_3Al-SO_4-LDHs	−2.86	2.34
Ni_3Al-$C_6H_5SO_3$-LDHs	−2.44	2.92
Ni_3Al-$C_{12}H_{25}SO_3$-LDHs	−3.84	2.60

https://doi.org/10.1021/acsomega.2c05067
ACS Omega 2022, 7, 39169−39180

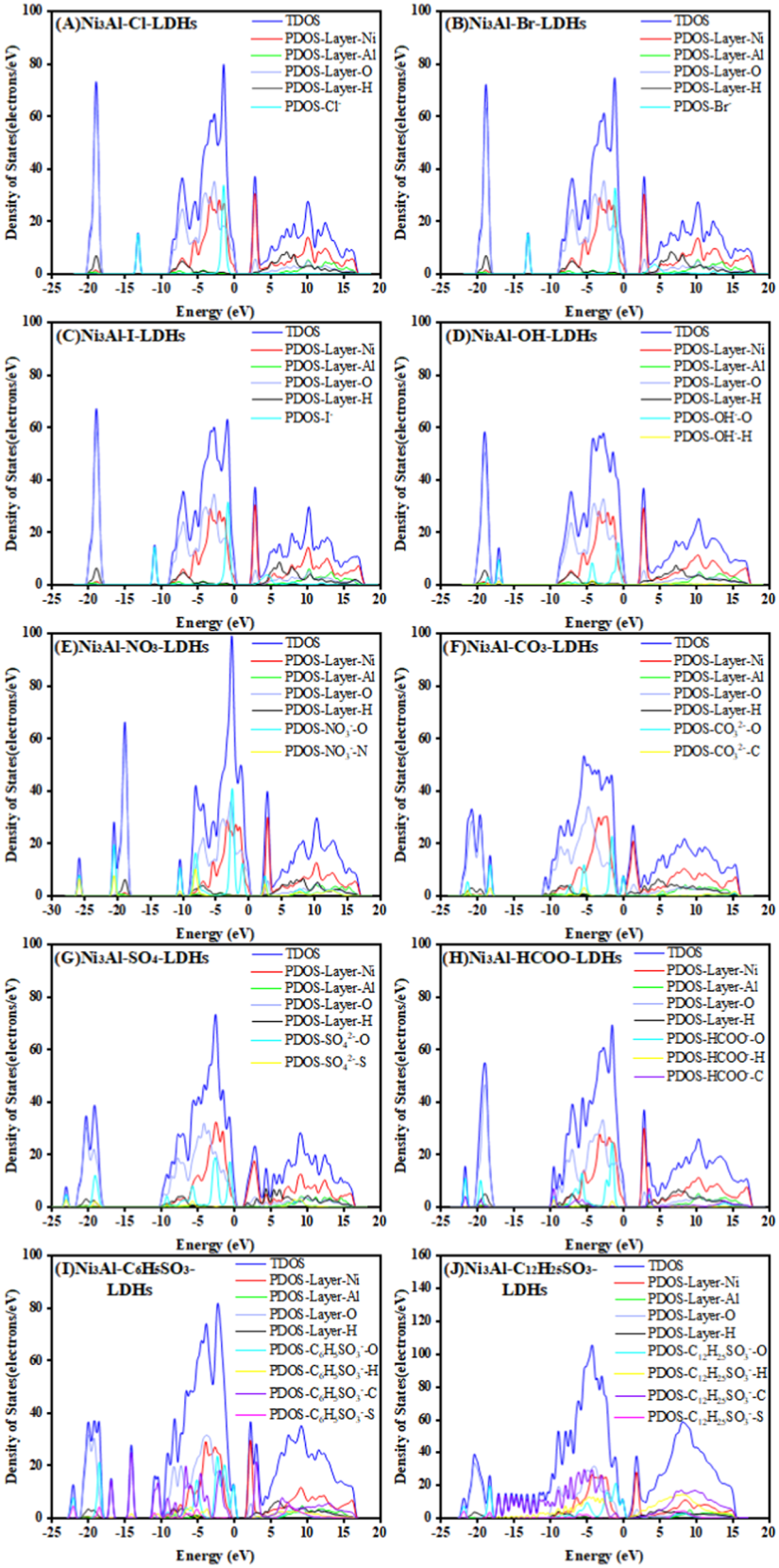

Figure 6. Density of states plots for different interlayer anion Ni_3Al-A-LDH (A = Cl^-, Br^-, I^-, OH^-, NO_3^-, CO_3^{2-}, SO_4^{2-}, $HCOO^-$, $C_6H_5SO_3^-$, $C_{12}H_{25}SO_3^-$) model systems.

without anion insertion. This indicates that the charge transfer from anions to basal layers occurs in the LDH system and the structure undergoes electrostatic interaction between anions and basal layers.

https://doi.org/10.1021/acsomega.2c05067
ACS Omega 2022, 7, 39169−39180

3.3. Effect of the Interlayer Anions on the Density of States. The density of states (DOS) refers to an electron at a given level that is allowed to occupy the number of different states, i.e., the number of electron states per unit volume of energy. The bulk properties of the conductive solid depend on this function. DOS calculations can determine the general state distribution of the semiconductor as a function of energy and the distance between the energy bands. To further investigate the effect of intercalating anions on Ni_3Al-LDHs, the DOS of Ni^{2+}, Al^{3+}, and OH^- in the basal layer and the interlayer anions was calculated and is shown in Figure 6. It can be observed that the DOS is mainly composed of two parts, the valence band top (VBM) and the conduction band bottom (CBM). In different interlayer anions of Ni_3Al-LDHs, the VBM total DOS is obtained from the interlayer halogen anion orbitals, the interlayer anion oxygen orbitals, and the oxygen orbitals in the hydroxyl groups of the basal layer. In contrast, the total DOS of CBM is contributed mainly by the slab Ni orbitals. The hole between the VBM and the CBM is called the band gap, and the smaller the band gap, the easier it is for the electrons to enter the CBM from the VBM. From Figure 7, it can be observed that the

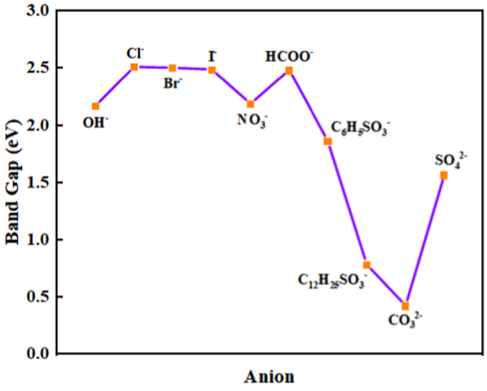

Figure 7. Comparison of the band gap values of different interlayer anion NiAl-A-LDH model systems.

band gap values of models intercalated by the different interlayer anions are in the order as follows: Cl^- (2.505 eV) > Br^- (2.497 eV) > I^- (2.482 eV) > $HCOO^-$ (2.477 eV) > NO_3^- (2.181 eV) > OH^- (2.163 eV) > $C_6H_5SO_3^-$ (1.854 eV) > SO_4^{2-} (1.561 eV) > $C_{12}H_{25}SO_3^-$ (0.779 eV) > CO_3^{2-} (0.421 eV). The band gap values of Ni_3Al-LDHs are smaller in the system of interlayer anions with two charges of CO_3^{2-} and SO_4^{2-} and long-chain anions $C_{12}H_{25}SO_3^-$. The partial density states contribution of O in the CO_3^{2-} intercalation system extends the conduction band region of the total DOS to the lower energy region, causing a weakening peaklet to arise near the Femi energy level, indicating a better conductivity. The partial density states peak of O in the SO_4^{2-} intercalation system is located at the upper end of the valence band, causing the valence band region to move to the higher energy region, resulting in a reduction of the band gap. It indicates that the higher the number of charges carried by the anion, the stronger its ability to provide electrons to the basal layer under the same charge density in the basal layer, which is unified with the analysis of binding energy and the charge population. When the interlayer anions are $C_{12}H_{25}SO_3^-$ and $C_6H_5SO_3^-$, due to the sudden increase in the number of its atoms, the charge number also undergoes a sudden increase, so that the lower the band gap value, the easier the electron migration occurs.

4. CONCLUSIONS

By the density functional theory of first principles, we calculated and analyzed the interlayer spacing, factors influencing the interlayer spacing, and the structural stability of 10 different intercalated anion Ni_3Al-A-LDH models and four different Ni_RAl-Cl-LDH models with different Ni−Al ratios. The results show the following.

(1) The order of the interlayer spacing of Ni_3Al-A-LDHs intercalated with different anions is OH^- < CO_3^{2-} < Cl^- < Br^- < I^- < $HCOO^-$ < SO_4^{2-} < NO_3^- < $C_6H_5SO_3^-$ < $C_{12}H_{25}SO_3^-$. The main factors affecting the interlayer spacing of Ni_3Al-A-LDHs are the interlayer anion structure, quantity, number of charges, the interlayer configuration, and the number of positive charges that carried basal layers. The hydrogen bond network formed between interlayer anions and basal layers results in anions with large differences in the size between the long axis and short axis tends to be arranged perpendicular to basal layers. The angles between the long-chain anions $C_{12}H_{25}SO_3^-$ and $C_6H_5SO_3^-$ and the basal layers are 86.094 and 87.089°, respectively. Interlayer spacing positively correlates with the projected size of the anion long axis in the direction perpendicular to the basal layer. The long-chain anion $C_{12}H_{25}SO_3^-$ intercalation system exhibits a maximum interlayer spacing of 24.262 Å, and the OH^- intercalation system obtains the smallest interlayer spacing of 7.447 Å. As the *R* value increases from 2 to 8, the interlayer spacing of Ni_RAl-Cl-LDHs gradually increases from 7.964 to 8.124 Å.

(2) The order of the binding energy between the interlayer anion and basal layer is CO_3^{2-} > SO_4^{2-} > OH^- > Cl^- > Br^- > I^- > $HCOO^-$ > NO_3^- > $C_{12}H_{25}SO_3^-$ > $C_6H_5SO_3^-$. The smaller the interlayer spacing, the higher the binding energy and the stronger the structural stability of LDHs. The factors affecting the structural stability mainly include the bond length and bond angle of the hydrogen bond and the charge interaction between the basal layer and interlayer anion. For interlayer monatomic anions Cl^-, Br^-, and I^- and anions of comparable size in each direction SO_4^{2-}, the interlayer spacing is positively correlated with the interlayer anion diameter. The larger the difference between the long-axis and short-axis dimensions of the polyatomic anions, the more the anions tend to be arranged perpendicular to the basal layer. In the CO_3^{2-} intercalated system, the shorter the hydrogen bond length between basal layer and interlayer CO_3^{2-}, the closer the bond angle is to 180°. In addition, the more the charge transfer between the basal layer and CO_3^{2-}, the more the decrease of the basal layer population value, indicating that the structure is the most stable. The band gaps of Ni_3Al-LDHs intercalated with dianions and long-chain sulfonate anions are small, and the band gap of the CO_3^{2-} intercalated system is the smallest at 0.421 eV.

AUTHOR INFORMATION

Corresponding Authors

Xiaoliang Wang − *College of Materials Science and Engineering, Key Laboratory of Mineral High Value Conversion and Energy Storage Materials of Liaoning Province, Geology and Mineral Engineering Special Materials Professional Technology Innovation Center of Liaoning Province, Liaoning Technical*

https://doi.org/10.1021/acsomega.2c05067
ACS Omega 2022, 7, 39169−39180

University, Fuxin 123000, China; orcid.org/0000-0003-3508-856X; Phone: 13704181324; Email: ningke@163.com

Shaobin Yang − *College of Materials Science and Engineering, Key Laboratory of Mineral High Value Conversion and Energy Storage Materials of Liaoning Province, Geology and Mineral Engineering Special Materials Professional Technology Innovation Center of Liaoning Province, Liaoning Technical University, Fuxin 123000, China*; Phone: 13941862976; Email: lgdysb@163.com

Authors

Haonan Zhao − *College of Materials Science and Engineering, Key Laboratory of Mineral High Value Conversion and Energy Storage Materials of Liaoning Province, Geology and Mineral Engineering Special Materials Professional Technology Innovation Center of Liaoning Province, Liaoning Technical University, Fuxin 123000, China*

Leiming Chang − *College of Materials Science and Engineering, Key Laboratory of Mineral High Value Conversion and Energy Storage Materials of Liaoning Province, Geology and Mineral Engineering Special Materials Professional Technology Innovation Center of Liaoning Province, Liaoning Technical University, Fuxin 123000, China*

Zhenqiu Yu − *College of Materials Science and Engineering, Key Laboratory of Mineral High Value Conversion and Energy Storage Materials of Liaoning Province, Geology and Mineral Engineering Special Materials Professional Technology Innovation Center of Liaoning Province, Liaoning Technical University, Fuxin 123000, China*

Zhiwu Xiao − *College of Materials Science and Engineering, Key Laboratory of Mineral High Value Conversion and Energy Storage Materials of Liaoning Province, Geology and Mineral Engineering Special Materials Professional Technology Innovation Center of Liaoning Province, Liaoning Technical University, Fuxin 123000, China*

Shuwei Tang − *College of Materials Science and Engineering, Key Laboratory of Mineral High Value Conversion and Energy Storage Materials of Liaoning Province, Geology and Mineral Engineering Special Materials Professional Technology Innovation Center of Liaoning Province, Liaoning Technical University, Fuxin 123000, China;* orcid.org/0000-0002-3963-8031

Chuanhui Huang − *School of Mechanical and Electrical Engineering, Xuzhou University of Technology, Xuzhou 221111, China*

Jingxin Fan − *CCTEG China Coal Research Institute, Beijing 100013, China*

Complete contact information is available at: https://pubs.acs.org/10.1021/acsomega.2c05067

Notes

The authors declare no competing financial interest.

■ ACKNOWLEDGMENTS

The project was supported by the National Natural Science Foundation of China (51974152), Natural Science Foundation of Liaoning Province, China (2019-ZD-0033), and discipline innovation team of Liaoning Technical University (Nos. LNTU20TD-9, LNTU20TD-16).

■ REFERENCES

(1) Lv, M.; Liu, H. Photocatalytic Property and Structural Stability of CuAl-Based Layered Double Hydroxides. *J. Solid State Chem.* **2015**, *227*, 232−238.

(2) Guzmán-Vargas, A.; Vazquez-Samperio, J.; Oliver-Tolentino, M. A.; Ramos-Sánchez, G.; Flores-Moreno, J. L.; Reguera, E. Influence on the Electrocatalytic Water Oxidation of M^{2+}/M^{3+} Cation Arrangement in Nife LDH: Experimental and Theoretical DFT Evidences. *Electrocatalysis* **2017**, *8*, 383−391.

(3) Pan, X.; Zhang, M.; Liu, H.; Ouyang, S.; Ding, N.; Zhang, P. Adsorption Behavior and Mechanism of Acid Orange 7 and Methylene Blue on Self-Assembled Three-Dimensional MgAl Layered Double Hydroxide: Experimental and DFT Investigation. *Appl. Surf. Sci.* **2020**, *522*, No. 146370.

(4) Tavares, S. R.; Carvalho, C.; Mantovani, K. M.; Wypych, F.; Nakagaki, S.; Leitão, A. A. Adsorption of an Iron(III) Porphyrin onto a 2:1 Zn/Al-CO_3 Layered Double Hydroxide and Its Use as an Oxidation Catalyst with Different Counter Ions: An Experimental and DFT Study. *Appl. Clay Sci.* **2020**, *185*, No. 105410.

(5) Lee, J.; Rhee, S.; Jung, D. Y. Orientation-Controlled Assembly and Solvothermal Ion-Exchange of Layered Double Hydroxide Nanocrystals. *Chem. Commun.* **2003**, 2740−1.

(6) Miyata, S. Anion-Exchange Properties of Hydrotalcite-Like Compounds. *Clays Clay Miner.* **1983**, *31*, 305−311.

(7) Su, B.; Bei, Z.; Pei, H.; Xie, X.; Sun, Z.; Chen, Q.; Cao, H.; Liu, X. Generation of a Nanobody-Alkaline Phosphatase Heptamer Fusion for Ratiometric Fluorescence Immunodetection of Trace Alpha Fetoprotein in Serum. *Int. J. Biol. Macromol.* **2022**, *201*, 507−515.

(8) Lu, C.; Kim, T. H.; Bendix, J.; Abdelmoula, M.; Ruby, C.; Nielsen, U. G.; Bruun Hansen, H. C. Stability of Magnetic LDH Composites Used for Phosphate Recovery. *J. Colloid Interface Sci.* **2020**, *580*, 660−668.

(9) Laipan, M.; Xiang, L.; Yu, J.; Martin, B. R.; Zhu, R.; Zhu, J.; He, H.; Clearfield, A.; Sun, L. Layered Intercalation Compounds: Mechanisms, New Methodologies, and Advanced Applications. *Prog. Mater. Sci.* **2020**, *109*, No. 100631.

(10) Xu, Y.; Hao, Y.; Zhang, G.; Lu, Z.; Han, S.; Li, Y.; Sun, X. Room-Temperature Synthetic NiFe Layered Double Hydroxide with Different Anions Intercalation as an Excellent Oxygen Evolution Catalyst. *RSC Adv.* **2015**, *5*, 55131−55135.

(11) Wu, X.; Jiang, L.; Long, C.; Wei, T.; Fan, Z. Dual Support System Ensuring Porous Co-Al Hydroxide Nanosheets with Ultrahigh Rate Performance and High Energy Density for Supercapacitors. *Adv. Funct. Mater.* **2015**, *25*, 1648−1655.

(12) Wu, X.; Du, Y.; An, X.; Xie, X. Fabrication of NiFe Layered Double Hydroxides Using Urea Hydrolysis—Control of Interlayer Anion and Investigation on Their Catalytic Performance. *Catal. Commun.* **2014**, *50*, 44−48.

(13) Zhou, D.; Cai, Z.; Bi, Y.; Tian, W.; Luo, M.; Zhang, Q.; Zhang, Q.; Xie, Q.; Wang, J.; Li, Y.; et al. Effects of Redox-Active Interlayer Anions on the Oxygen Evolution Reactivity of NiFe-Layered Double Hydroxide Nanosheets. *Nano Res.* **2018**, *11*, 1358−1368.

(14) Wang, X. L.; Li, Z.; Zhang, J. Q.; Yan, H. Y.; Wang, C.; Wu, F. Q.; Tian, A. N.; Hong, X. D.; Dong, W.; Yang, S. B. Effect of Average Interlayer Spacing on Capacitance of NiMn Layered Double Hydroxide. *Chem. Eng. J.* **2020**, *398*, No. 125618.

(15) Prasad, B. E.; Kamath, P. V.; Vijayamohanan, K. Anion Exchange Reaction Potentials as Approximate Estimates of the Relative Thermodynamic Stabilities of Mg/Al Layered Double Hydroxides Containing Different Anions. *Langmuir* **2011**, *27*, 13539−13543.

(16) Hunter, B. M.; Hieringer, W.; Winkler, J. R.; Gray, H. B.; Müller, A. M. Effect of Interlayer Anions on [NiFe]-LDH Nanosheet Water Oxidation Activity. *Energy Environ. Sci.* **2016**, *9*, 1734−1743.

(17) Wang, Y.; Yang, W.; Chen, C.; Evans, D. G. Fabrication and Electrochemical Characterization of Cobalt-Based Layered Double Hydroxide Nanosheet Thin-Film Electrodes. *J. Power Sources* **2008**, *184*, 682−690.

(18) Lu, Z.; Zhu, W.; Lei, X.; Williams, G. R.; O'Hare, D.; Chang, Z.; Sun, X.; Duan, X. High Pseudocapacitive Cobalt Carbonate Hydroxide

Films Derived from Coal Layered Double Hydroxides. *Nanoscale* **2012**, *4*, 3640−3643.
(19) Fan, G.; Li, F.; Evans, D. G.; Duan, X. Catalytic Applications of Layered Double Hydroxides: Recent Advances and Perspectives. *Chem. Soc. Rev.* **2014**, *43*, 7040−7066.
(20) Tan, Z.; Luo, X.; Wei, T.; Zhang, F.; Lv, Y.; Chen, L.; Shi, Y. In Situ Formation of NiAl-Layered Double Hydroxide with a Tunable Interlayer Spacing in a Confined Impinging Jet Microreactor. *Energy Fuels* **2020**, *34*, 8939−8946.
(21) Li, Y.; Huang, B.; Zhao, X.; Luo, Z.; Liang, S.; Qin, H.; Chen, L. Zeolitic Imidazolate Framework-L-Assisted Synthesis of Inorganic and Organic Anion-Intercalated Hetero-Trimetallic Layered Double Hydroxide Sheets as Advanced Electrode Materials for Aqueous Asymmetric Super-Capacitor Battery. *J. Power Sources* **2022**, *527*, No. 231149.
(22) Bouragba, F. Z.; Elhatimi, W.; Lahkale, R.; Moujahid, E. M.; Sabbar, E. Effect of Intercalated Anions on the Electrical and Dielectric Properties of NiAl-X Layered Double Hydroxide: Investigation by Impedance Spectroscopy. *Bull. Mater. Sci.* **2020**, *43*, No. 90.
(23) Bao, W.; Tian, H.; Jiang, Y.; Zhu, K.; Zhang, R.; Tan, Y.; Li, W.; Yu, Z.; Wang, L. Controlled Preparation of Ni−Al LDH−NO_3 by a Dual-Anion Intercalating Process for Supercapacitors. *Ionics* **2019**, *25*, 3859−3866.
(24) Lv, H.; Rao, H.; Liu, Z.; Zhou, Z.; Zhao, Y.; Wei, H.; Chen, Z. NiAl Layered Double Hydroxides with Enhanced Interlayer Spacing Via Ion-Exchange as Ultra-High Performance Supercapacitors Electrode Materials. *J. Energy Storage* **2022**, *52*, No. 104940.
(25) Arulmurugan, P.; Manikandan, N. A.; Pugazhenthi, G. Synthesis and Characterization of Polystyrene (Ps)/Modified Ni-Al LDH Nanocomposite: Role of Composition, Modifier and Synthesis Route of Layered Double Hydroxides (LDH). *Macromol. Symp.* **2018**, *382*, No. 1800078.
(26) Ding, S.; Du, X.; Yang, Y.; Wang, P.; Zhang, Z.; Hao, X.; Peng, C.; Guan, G. Theoretical and Experimental Investigations of the Electronic/Ionic Conductivity and Deprotonation of $Ni_{3-X}Co_XAl$-LDHs in an Electrochemical Energy Storage System. *Phys. Chem. Chem. Phys.* **2018**, *20*, 17313−17323.
(27) Costa, D. G.; Rocha, A. B.; Souza, W. F.; Chiaro, S. S.; Leitao, A. A. Ab Initio Simulation of Changes in Geometry, Electronic Structure, and Gibbs Free Energy Caused by Dehydration of Hydrotalcites Containing Cl^- and CO_3^{2-} Counteranions. *J. Phys. Chem. B* **2011**, *115*, 3531−3537.
(28) Liu, H. M.; Zhao, X. J.; Zhu, Y. Q.; Yan, H. DFT Study on MgAl-Layered Double Hydroxides with Different Interlayer Anions: Structure, Anion Exchange, Host-Guest Interaction and Basic Sites. *Phys. Chem. Chem. Phys.* **2020**, *22*, 2521−2529.
(29) Costa, D. G.; Rocha, A. B.; Diniz, R.; Souza, W. F.; Chiaro, S. S. X.; Leitão, A. A. Structural Model Proposition and Thermodynamic and Vibrational Analysis of Hydrotalcite-Like Compounds by DFT Calculations. *J. Phys. Chem. C* **2010**, *114*, 14133−14140.
(30) Xia, S.; Qian, M.; Zhou, X.; Meng, Y.; Xue, J.; Ni, Z. Theoretical and Experimental Investigation into the Photocatalytic Degradation of Hexachlorobenzene by Zncr Layered Double Hydroxides with Different Anions. *Mol. Catal.* **2017**, *435*, 118−127.
(31) Zhao, X. J.; Zhu, Y. Q.; Xu, S. M.; Liu, H. M.; Yin, P.; Feng, Y. L.; Yan, H. Anion Exchange Behavior of $M^{(II)}Al$ Layered Double Hydroxides: A Molecular Dynamics and DFT Study. *Phys. Chem. Chem. Phys.* **2020**, *22*, 19758−19768.
(32) Xu, S.-M.; Pan, T.; Dou, Y.-B.; Yan, H.; Zhang, S.-T.; Ning, F.-Y.; Shi, W.-Y.; Wei, M. Theoretical and Experimental Study on Miimiii-Layered Double Hydroxides as Efficient Photocatalysts toward Oxygen Evolution from Water. *J. Phys. Chem. C* **2015**, *119*, 18823−18834.
(33) Kameda, T.; Yamazaki, T.; Yoshioka, T. Preparation and Characterization of Mg−Al Layered Double Hydroxides Intercalated with Benzenesulfonate and Benzenedisulfonate. *Microporous Mesoporous Mater.* **2008**, *114*, 410−415.
(34) Xu, Q.; Ni, Z.-m.; Mao, J.-h. First Principles Study of Microscopic Structures and Layer-Anion Interactions in Layered Double Hydroxides Intercalated Various Univalent Anions. *J. Mol. Struct.: THEOCHEM* **2009**, *915*, 122−131.
(35) Ernzerhof, M.; Scuseria, G. E. Assessment of the Perdew−Burke−Ernzerhof Exchange-Correlation Functional. *J. Chem. Phys.* **1999**, *110*, 5029−5036.
(36) Ceperley, D. M.; Alder, B. J. Ground State of the Electron Gas by a Stochastic Method. *Phys. Rev. Lett.* **1980**, *45*, 566−569.
(37) Perdew, J. P.; Yue, W. Accurate and Simple Density Functional for the Electronic Exchange Energy: Generalized Gradient Approximation. *Phys. Rev. B* **1986**, *33*, 8800−8802.
(38) Xu, S.-M.; Yan, H.; Wei, M. Band Structure Engineering of Transition-Metal-Based Layered Double Hydroxides toward Photocatalytic Oxygen Evolution from Water: A Theoretical−Experimental Combination Study. *J. Phys. Chem. C* **2017**, *121*, 2683−2695.
(39) Moraes, P. I. R.; Tavares, S. R.; Vaiss, V. S.; Leitão, A. A. Ab Initio Study of Layered Double Hydroxides Containing Iron and Its Potential Use as Fertilizer. *J. Phys. Chem. C* **2016**, *120*, 9965−9974.
(40) Tavares, S. R.; Wypych, F.; Leitão, A. A. DFT Study of the Intercalation of Layered Double Hydroxides and Layered Hydroxide Salts with Dodecylsulfate and Dodecylbenzene Sulfonate: Exfoliation and Hydration properties. *Appl. Clay Sci.* **2017**, *143*, 107−114.
(41) Ding, D.; Song, X.; Wei, C.; Hu, Z.; Liu, Z. Efficient Sorptive Removal of F-53B from Water by Layered Double Hydroxides: Performance and Mechanisms. *Chemosphere* **2020**, *252*, No. 126443.
(42) Cursino, A. C. T.; Lisboa Fda, S.; Pyrrho Ados, S.; de Sousa, V. P.; Wypych, F. Layered Double Hydroxides Intercalated with Anionic Surfactants/Benzophenone as Potential Materials for Sunscreens. *J. Colloid Interface Sci.* **2013**, *397*, 88−95.
(43) Zhao, X.-J.; Xu, S.-M.; Zhong, Y.; Chen, Z.-R.; Yin, P.; Miao, Y.-C.; Guo, J.-Y.; Zhang, W.; Jie, Y.; Yan, H. Theoretical Study on Photocatalytic CO_2 Reduction to CO and CH_4 over $M_2^{(II)}M^{(II/IV)}$-Layered Double Hydroxides. *J. Phys. Chem. C* **2022**, *126*, 1356−1365.
(44) Yan, H.; Wei, M.; Ma, J.; Duan, X. Density Functional Theory Study on the Influence of Cation Ratio on the Host Layer Structure of Zn/Al Double Hydroxides. *Particuology* **2010**, *8*, 212−220.
(45) Yoosefian, M.; Mola, A. Solvent Effects on Binding Energy, Stability Order and Hydrogen Bonding of Guanine−Cytosine Base Pair. *J. Mol. Liq.* **2015**, *209*, 526−530.
(46) Lebrun, N.; Mahe, F.; Lamiot, J.; Foulon, M.; Petit, J. C.; Prevost, D. Kinetic Behaviour Investigations and Crystal Structure of Nitric Acid Dihydrate. *Acta Crystallogr., Sect. B: Struct. Sci.* **2001**, *57*, 27−35.
(47) Uno, T.; Kuwae, A.; Saito, Y.; Machida, K. Normal Vibrations of Benzenesulfonate and Benzene-d5-Sulfonate Ions. *Bull. Chem. Soc. Jpn.* **1975**, *48*, 2231−2235.
(48) Gu, Y.; Chen, S.; Liu, H.; Wang, Y.; Zhou, P. Effect of Monovalent Anions on Cationic Gemini Micro-Emulsion. *Chin. J. Chem. Eng.* **2018**, *26*, 2636−2640.
(49) Costa, D. G.; Rocha, A. B.; Souza, W. F.; Chiaro, S. S. X.; Leitão, A. A. Comparative Structural, Thermodynamic and Electronic Analyses of Zn-Al-A^{n-} Hydrotalcite-Like Compounds (A^{n-} = Cl^-, F^-, Br^-, OH^-, CO_3^{2-} or NO_3^-): An Ab Initio Study. *Appl. Clay Sci.* **2012**, *56*, 16−22.
(50) Barbosa, A. C. d. A.; Fonseca, C. G.; Wypych, F.; Leitão, A. A. Structural Analysis of Dehydrated Gibbsite-Based Layered Double Hydroxides Li−Al−X (X = F−, Cl−, Br−, I−, OH−, NO3−, CO32−, and SO42−) by DFT Calculations. *New J. Chem.* **2020**, *44*, 10137−10145.
(51) Nobeli, I.; Laskowski, R. A.; Valdar, W. S. J.; Thornton, J. M. On the Molecular Discrimination between Adenine and Guanine by Proteins. *Nucleic Acids Res.* **2001**, *29*, 4294−4309.
(52) Arunan, E.; Desiraju, G. R.; Klein, R. A.; Sadlej, J.; Scheiner, S.; Alkorta, I.; Clary, D. C.; Crabtree, R. H.; Dannenberg, J. J.; et al. Definition of the Hydrogen Bond (Iupac Recommendations 2011). *Pure Appl. Chem.* **2011**, *83*, 1637−1641.
(53) Ni, Z.-M.; Li, Y.; Shi, W.; Xue, J. L.; Liu, J. Supramolecular Structure, Electronic Property and Stability of Ni-Mg-Al Layered Double Hydroxides. *Acta Phys.-Chim. Sin.* **2012**, *28*, 2051−2056.

https://doi.org/10.1021/acsomega.2c05067
ACS Omega 2022, 7, 39169−39180